Mon. Not. R. Astron. Soc. **263,** 749–766 (1993)

Grain mantles in the Taurus dark cloud

R. G. Smith,[1]★ K. Sellgren[2]★† and T. Y. Brooke[3]★

[1] *Department of Physics, University College, University of New South Wales, Canberra, ACT 2600, Australia*
[2] *Department of Astronomy, Ohio State University, 174 West 18th Avenue, Columbus, OH 43210, USA*
[3] *Jet Propulsion Laboratory, MS 169-237, 4800 Oak Grove Drive, Pasadena, CA 91109, USA*

Accepted 1993 February 1. Received 1993 January 27; in original form 1992 October 19

ABSTRACT

We have obtained low-resolution ($\lambda/\Delta\lambda \sim 160$) 3-μm spectra of a selection of field stars lying behind the Taurus dark cloud. Several of these stars have abnormal extinction laws, which are best characterized by $A_K \leq 0.27E(J-K)$ and $A_V \leq 5.4E(J-K)$. We find a very good correlation between A_V and $\tau_{3.05}$ (the H_2O ice feature), confirming a previous result, and between A_V and $\tau_{3.45}$ (the long-wavelength wing), yielding the ratios $\tau_{3.05}/A_V = 0.059 \pm 0.003$ and $\tau_{3.45}/A_V = 0.0077 \pm 0.0005$. The threshold extinctions for the H_2O ice band and the long-wavelength wing are found to be the same, within the uncertainties, at $A_{V_0} = 2.6$. The fact that these thresholds are the same means that the long-wavelength wing cannot be a result of a highly refractory hydrocarbon residue. The lack of substructure in the long-wavelength wing also argues against a hydrocarbon origin for the wing.

By interpreting the H_2O ice feature with a model employing silicate and graphite grain cores that follow a power-law size distribution, we find that the ice band observations can only be fitted by models in which either (i) only the largest grains have significant ice mantles, or (ii) there are two grain populations throughout the cloud, one of 'bare' grains and one of grains that have a constant ice mantle thickness of 0.35 ± 0.05 μm. In the latter model, we estimate the ratio of bare to mantled grains to be $\sim 3 \times 10^4$:1. Both models, combined with the observed $\tau_{3.05}/A_V$ ratio, imply that 8–9 per cent of the oxygen is depleted on to the grains as H_2O ice mantles. We discuss a number of mechanisms for the production of the H_2O ice and long-wavelength wing thresholds, and conclude that photodesorption is the most likely means of prevention of H_2O ice mantle formation near the cloud edges. Photodesorption, combined with a clumpy cloud structure, also naturally explains the bare/mantled grain distribution, as UV photons penetrating into the cloud prevent ice mantle formation everywhere except within dense clumps.

Key words: molecular processes – stars: late-type – ISM: clouds – dust, extinction – infrared: general.

1 INTRODUCTION

Icy grain mantles are an almost ubiquitous feature of dust in dense molecular clouds, sufficiently common that we can consider their use as a tool to probe the chemical and physical environment of the dust inside these clouds. The potential for this can be seen in the work of Whittet et al. (1983, 1988, 1989) and Whittet, Longmore & McFadzean (1985) on the nearby Taurus dark cloud: they have detected H_2O and CO ices throughout most of the cloud. However, although Taurus has been the subject of a great deal of study, there is still substantial uncertainty about the composition and physical state of the dust grains and their mantles. Observations of the 3-μm H_2O ice band are an effective means of resolving much of this uncertainty – a point we hope to demonstrate in this paper.

In dense molecular clouds like Taurus, absorption in the 3-μm region is typically characterized by a feature with a peak absorption near 3.1 μm. This feature is in general not symmetric: there is additional absorption stretching from about 3.2 to 3.6 μm, the so-called 'long-wavelength wing'. The 3.1-μm absorption itself is firmly identified with H_2O ice

★ Visiting Astronomer at the Infrared Telescope Facility, operated by the University of Hawaii under contract to the National Aeronautics and Space Administration.
† Alfred P. Sloan Foundation Research Fellow.

on or in the dust grains, but the origin of the long-wavelength wing has not yet been definitely established. Among the proposals are (i) extinction by large ice-coated grains (Léger et al. 1983), (ii) absorption produced by $H_2O \cdot NH_3$ mixtures (Merrill, Russell & Soifer 1976), and (iii) some form of hydrocarbon (e.g. Duley & Williams 1981; Schutte & Greenberg 1986; Sandford et al. 1991).

One step towards the settling of this question would be to determine the volatility of the material responsible for the long-wavelength wing, relative to H_2O and CO ices. Whittet et al. (1988, 1989) find that the column densities of H_2O and CO ices correlate well with the total visual extinction, A_V, along most lines of sight in Taurus, but that no H_2O ice exists on the grains below a threshold A_V of ~ 3.3, while no CO ice exists below a threshold A_V of ~ 5.3. Whittet et al. suggest that the A_V thresholds reflect the volatility of the ices, which are destroyed by visible/UV radiation reaching the grains near the edges of the cloud. This suggests that a determination of the threshold A_V for the long-wavelength wing could put constraints on the material giving rise to this feature. Complex hydrocarbons, for example, which have been proposed as an explanation for a feature found near 3.4 μm in the diffuse interstellar medium (Schutte & Greenberg 1986; Sandford et al. 1991), are clearly able to survive a much harsher radiation environment than is likely to be present in the Taurus dark cloud. Such materials would be expected to remain on the grains even after the H_2O ice has disappeared. These complex hydrocarbons are believed to form through UV photolysis of simple ices (e.g. H_2O, NH_3, CH_4, CH_3OH, etc.) in grain mantles. This suggestion is well supported by the good match between the diffuse interstellar medium (ISM) 3.4-μm feature and the laboratory spectra of the *residues* produced when mixtures of simple molecular ices are exposed to UV radiation (e.g. Sandford et al. 1991). If photolysis of the icy grain mantles in Taurus can lead to a 3.4-μm absorption feature like that seen in the diffuse ISM, then, by examining the long-wavelength wing in the low-A_V Taurus sources (i.e. where external UV radiation is most likely to reach the grain mantles), we might see a change in the strength of the wing relative to the 3.1-μm H_2O ice feature, or changes in the shape of the wing, or both, as a function of A_V.

We have reobserved a selection of the Taurus background field stars from the sample of Whittet et al. (1988), with both higher resolution and as high a signal-to-noise ratio as we could reasonably achieve, to try to answer these questions. Our specific goals are (i) to examine the correlation between A_V and the optical depth in the H_2O ice band and long-wavelength wing, (ii) to determine the threshold extinction below which the long-wavelength wing disappears, and hence to determine the volatility of the material responsible for the wing, (iii) to search for evidence of grain mantle photolysis, and (iv) to use models of the ice band to estimate the most probable size distribution of the ice mantles in the Taurus cloud.

2 OBSERVATIONS

The observations of the Taurus field stars reported here were made with the NASA Infrared Telescope Facility (IRTF) during 1989 December and 1991 January, using the 32-element Cooled Grating Array Spectrometer (CGAS: Tokunaga, Smith & Irwin 1987), fitted with a 2.7-arcsec aperture.

All of the observations were made using CGAS Grating A (75 lines mm^{-1}) over the spectral range 2.0 to 3.8 μm. Wavelength calibration was achieved by using lines from an argon lamp, with an estimated accuracy of ~ 10 per cent of a resolution element. The wavelength resolution $\Delta\lambda$ varies from 0.0190 to 0.0196 μm between 2.0 and 3.8 μm. In the vicinity of the 3.1-μm ice feature, $\Delta\lambda = 0.0195$ μm, resulting in a spectral resolution, $\lambda/\Delta\lambda$, of ~ 160. Detectors 1, 2 and 32 in CGAS are not reliable, and data from these detectors have been discarded. Detector 13 is unreliable under low-background conditions, so the 2-μm data from this detector have also been discarded. Coverage of the full wavelength range from 2.0 to 3.8 μm required four separate grating settings, after allowing for a 6–8 detector overlap for normalization. This normalization was necessary because seeing and tracking drifts can cause shifts in the absolute level of individual observations and sometimes tilts of up to ~ 6 per cent. Since there are typically several observations of each spectral segment, before co-adding individual observations the flux level of each one was normalized to the average flux level of that segment, and the slope of each observation was forced to match that of the majority of the observations. The four separate spectral segments were then combined into one complete spectrum. Each spectral segment was divided by the spectrum of a standard star and multiplied by a blackbody function with a temperature appropriate for that star. Although several standard stars were observed during the course of this work, one standard star, BS 1497 (spectral type B3V), was used for all of the observations, primarily because this provided the most accurate way to intercompare the spectra. A comparison between BS 1497 and the other standards showed that there were no unusual features in the BS 1497 spectrum. BS 1497 was observed often enough that the maximum difference in airmass between it and the programme stars was never more than 0.05, and thus no extinction corrections have been applied to the spectra. The spectra of the complete sample of 11 objects are shown in Fig. 1; Elias 16 has already been observed by Smith, Sellgren & Tokunaga (1989), and the spectrum shown in Fig. 1 is taken from that work. Because the standard star is of early spectral type (B3V), the spectra in Fig. 1 show features near 3.74, 3.04 and 2.16 μm, which arise from Pfγ, H I 10–5 and Brγ absorption respectively, in this star. There is probably also a Pfδ feature near 3.30 μm, but this is difficult to separate from the effects of poor cancellation of the strong telluric methane absorption in the same region.

3 RESULTS

3.1 Optical depths and spectral types

In order to convert the observed spectra to optical depths, it was necessary to fit a continuum to each spectrum. For the early-type stars, the continuum was assumed to be well represented by a hot blackbody. For the late-type stars, the spectral types listed by Whittet et al. (1988) were initially used to select spectra of stars of similar spectral type from the studies of Merrill & Stein (1976), Strecker, Erickson & Witteborn (1979) and Scargle & Strecker (1979). These spectra were then reddened to fit the observed spectra in Fig.

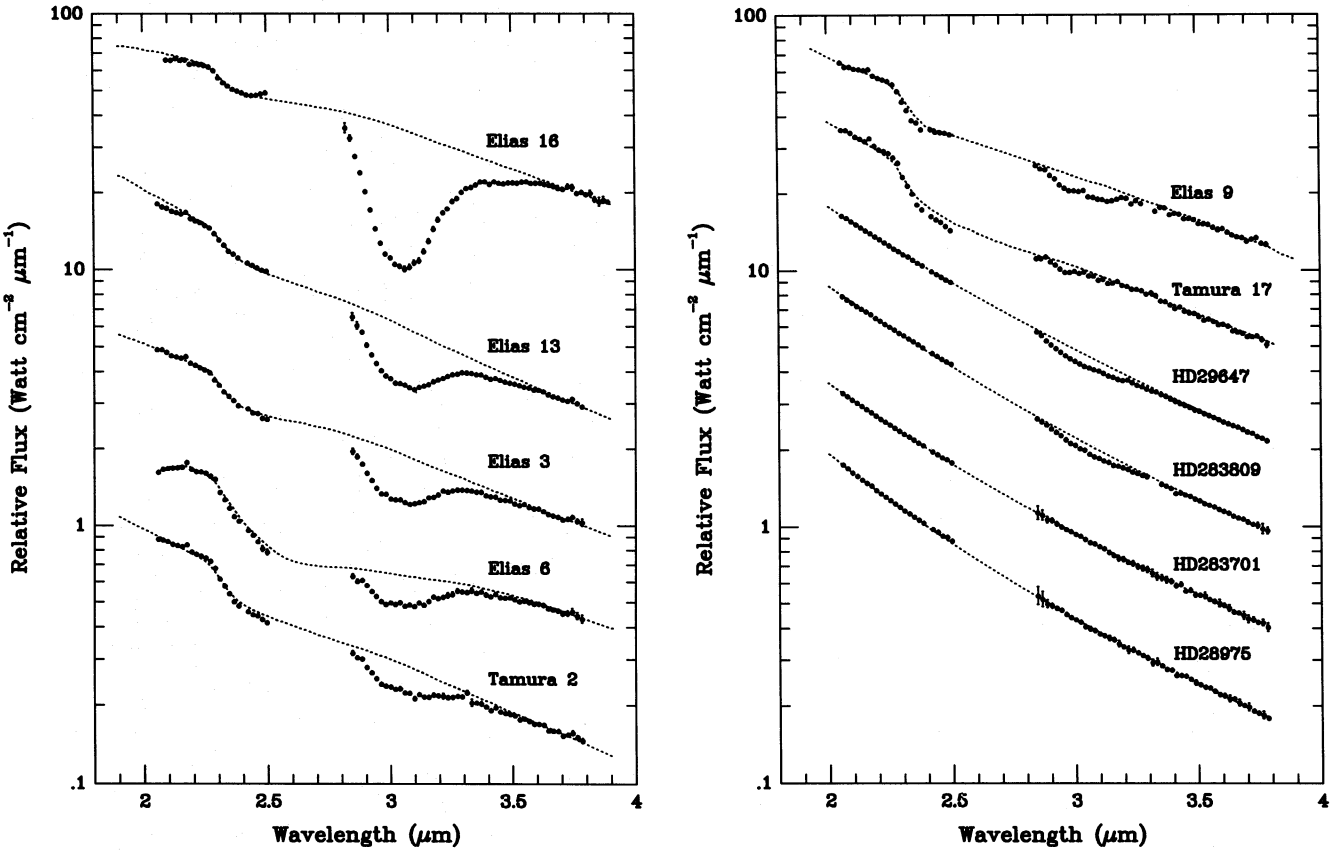

Figure 1. Low-resolution spectra ($\lambda/\Delta\lambda \sim 160$ at 3.1 μm) of the sample of Taurus field stars (error bars are $\pm 1\sigma$), plotted on a relative flux scale, where individual spectra have been shifted in flux by an arbitrary amount. The dashed lines represent an estimate of the continuum for each source, based on reddened normal stellar spectra for the late-type stars and reddened blackbodies for the early-type stars (i.e. the HD stars).

1. Where this did not provide an acceptable fit, another slightly different spectral type was chosen, the process continuing until a satisfactory fit had been achieved. Although in most cases the nominal spectral type provided the best fit, this was not always true, in which case the fit was then used to assign what was considered to be the more appropriate spectral type. (Note that only the late spectral types have been modified in this way, since only they have spectral features in this wavelength range that are sensitive to spectral type, i.e. photospheric CO and OH absorption.) The assigned spectral types for the entire sample are listed in Table 1. The best-fitting continuum in each case was then used to convert the observed fluxes to an optical depth scale, shown in Fig. 2(a) for the late-type stars and in Fig. 2(b) for the early-type stars. If the true spectral type obviously lay between the spectral types we had available for comparison, an interpolated continuum (not shown) was used to determine the optical depths in the 2.8–3.8 μm range.

The optical depth at 3.05 μm was taken to be representative of the strength of the H_2O ice absorption, while the optical depth at 3.45 μm was taken as a measure of the strength of the long-wavelength wing (an average of three points was used here to improve the signal-to-noise ratio of the estimate because of the intrinsic weakness of the feature). The 3.05- and 3.45-μm optical depths estimated for each spectrum are listed in Table 1. The presence of a H I 10–5 feature near 3.04 μm in the spectra of the late-type stars (resulting from absorption in the standard star) can introduce a systematic error in the 3.05-μm optical depth estimate. To get around this problem, an ice-coated grain model was fitted to all spectra, as shown in Fig. 2 (for details of the model, see Section 4), and the peak optical depth of the model was then used to estimate the H_2O ice absorption strength. This has the additional advantage of providing an improved estimate of $\tau_{3.05}$ in those cases where the signal-to-noise ratio is poor, because the model fit is based on many more points than the few around 3.05 μm.

The models in Fig. 2 show that H_2O ice contributes to the absorption near 3.45 μm. For this reason, we have included an extra column in Table 1, which lists the 3.45-μm optical depth *after* subtracting the H_2O ice contribution (as determined by the best-fitting model). We note, however, that this optical depth estimate is model-dependent.

There are some differences apparent when comparing $\tau_{3.05}$ in Table 1 with the values of $\tau_{3.0}$ determined by Whittet et al. (1988) for the same objects, and these differences are greater than can be accounted for by the small wavelength difference between the points at which the optical depths were measured. We attribute these to differences in the choice of continuum. As has already been explained, the optical depths in Table 1 have been determined relative to the best-fitting stellar continuum, reddened to fit the observations over the wavelength range 2.0–3.8 μm. In contrast, Whittet et al. (1988) were only able to fit longwards of 2.3

Table 1. Assigned spectral types, extinctions and measured optical depths.

Source	Spectral Type	E(J–K)	A_V (mag.)	$\tau_{3.05}$	$\tau_{3.45}$	$\tau_{3.45}$ [a]	Ref. [b]
Elias 16	K2 III	4.42	23.9 ±0.2	1.257	0.162	0.138	1,*
Elias 13	K2 III	2.24	12.1 ±0.2	0.540	0.075	0.065	1,*
Elias 3	K4 III	1.62	8.7 ±0.3	0.425	0.051	0.042	1,*
Tamura 2	M2 III	1.25	6.8 ±0.5	0.255	0.028	0.028	2,*
Elias 6	M7 III	1.25	6.8 ±0.2	0.273	0.042	0.037	1,*
Elias 9	M4 III	0.96	5.2 ±0.2	0.155	0.009	0.007	1,*
Tamura 17	M8 III	0.74	4.0 ±0.5	0.055	0.008	0.007	2,*
HD29647	B7 IV	0.67	3.6 ±0.3	0.108	0.019	0.017	3,5
HD283809	B3 V	1.00	5.4 ±1.0	0.075	0.013	0.011	4,4
HD283701	A0 V	0.36	2.5 ±0.9	0.010[c]	0.002[c]	...	3,3
HD28975	A3 (V)	0.31	1.9 ±0.5	0.019[c]	−0.003[c]	...	6,6

Notes to table.
Uncertainties in *all* optical depths are estimated to be ±0.01. The formal value for the best-fitting optical depth is given, even when less than 0.03.
[a]Optical depth at 3.45 μm after subtracting the H_2O ice contribution (determined from the best fit of model 4).
[b]Infrared photometry (first reference) and spectral types (second reference) from (1) Elias (1978), (2) Tamura et al. (1987), (3) Straižys et al. (1982), (4) Straižys et al. (1985), (5) Crutcher (1985), (6) Vrba & Rydgren (1985), *this work.
[c]The 3.45-μm optical depth corrected for the H_2O ice contribution at 3.45 μm is not given for sources without a 3σ detection of H_2O ice absorption.

μm, the short-wavelength limit of their spectra. It is possible that this could have affected their estimates of the peak ice band optical depth in some cases.

3.2 The reddening law and A_V

The sample of stars in Fig. 1 contains both late- and early-type stars, selected from the study of Whittet et al. (1988), and basically chosen to span as wide a range in A_V as possible. However, to obtain reasonably accurate estimates of A_V, which is useful in judging how much external UV radiation is reaching the grain mantles, we need to adopt a reddening law, typically given in the form $R = A_V/E(B-V)$, for the Taurus cloud.

While the available photometry does not cover a wide enough wavelength range to allow us to evaluate R explicitly for the late-type stars, the two early-type stars that have distinct ice absorption features in their spectra, HD 29647 and 283809, both have R-values of 3.5, whereas the two that do not, HD 28975 and 283701, have R-values of 2.8 and 2.9 respectively (see Straižys, Wisniewski & Lebofsky 1982; Straižys, Černis & Hayes 1985; Vrba & Rydgren 1985). The obvious interpretation of this is that the presence of ice mantles on the grains has altered the extinction law.

To determine whether it might be reasonable to adopt $R = 3.5$ for the entire sample, we first assumed 'normal' extinction (based on the standard van de Hulst extinction curve: see Johnson 1968), and dereddened the observed K magnitudes (for the late-type stars) using $A_K = 0.6E(J-K)$ and the V magnitudes (for the early-type stars) using $A_V = 6.3E(J-K)$. These apparent magnitudes were then compared with the calculated apparent K and V magnitudes

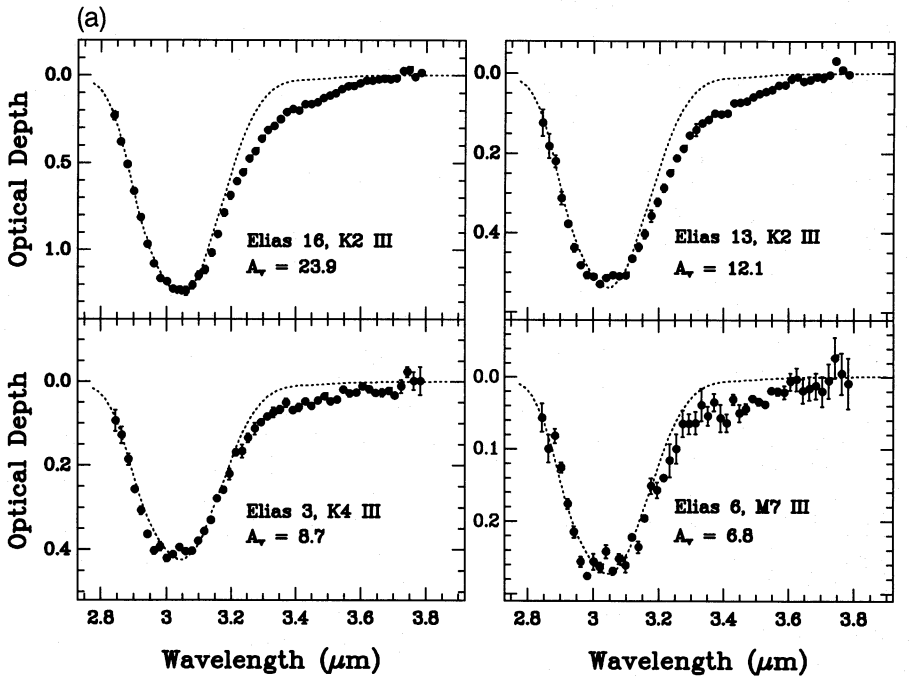

Figure 2. The spectra of (a) the late-type stars, and (b) the early-type stars, plotted in terms of optical depth (error bars are ±1σ). The dashed lines in each spectrum show the calculated extinction for an H_2O ice-coated grain model (model 4, $a_{th} = 0.35$ μm).

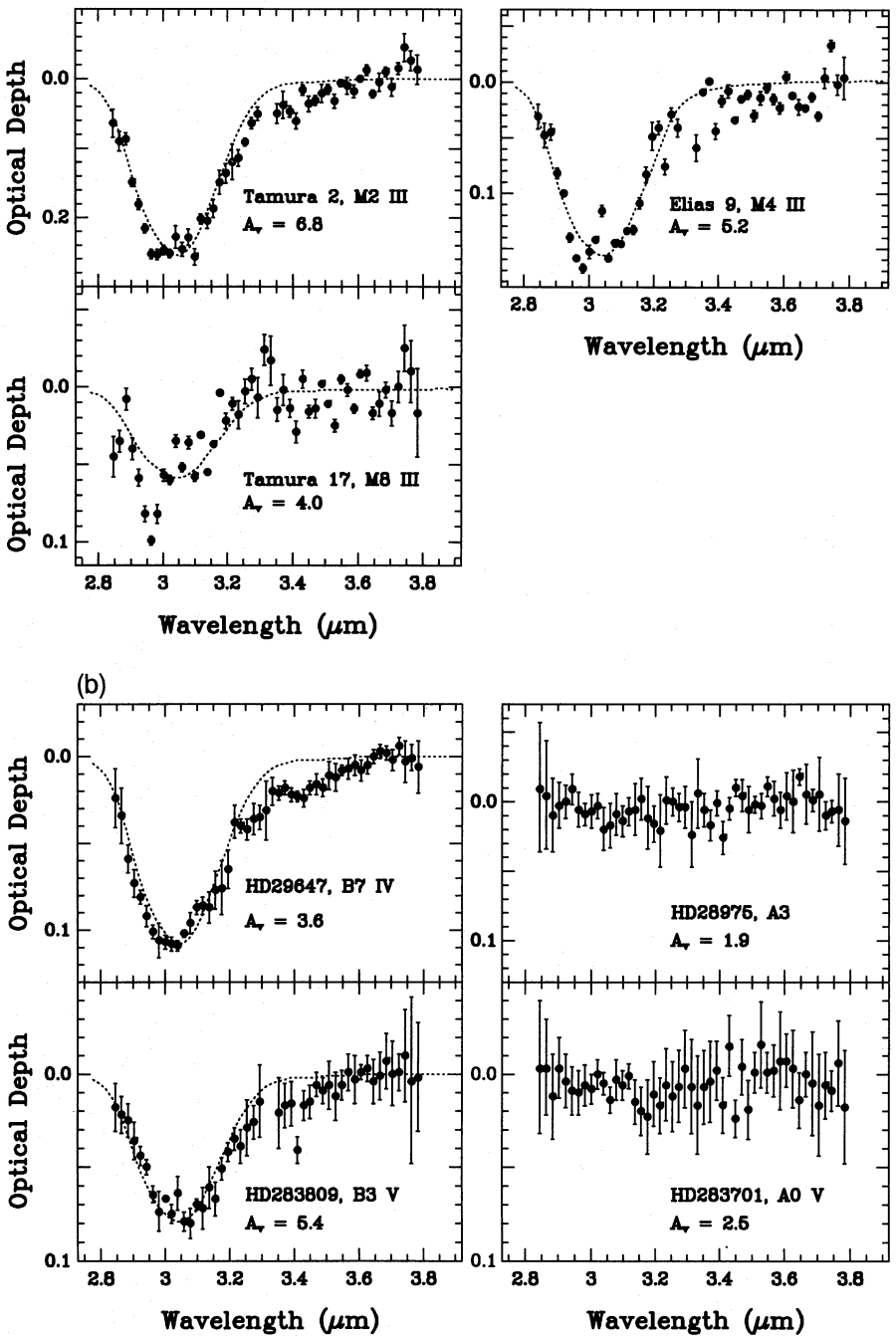

Figure 2 – *continued*

for stars of the same spectral type lying at the nominal distance of the Taurus cloud, ~140 pc (Elias 1978). The absolute K magnitudes were calculated from the absolute V magnitudes listed by Allen (1973), combined with the intrinsic $(V-K)$ colours from Frogel et al. (1978) for the late-type stars and from Whittet & van Breda (1980) for the early-type stars. These were then converted to apparent magnitudes for stars at a distance of 140 pc. Straižys & Meištas (1980) find a sharp increase in extinction in the direction of Taurus at ~140 pc, consistent with the nominal cloud distance and showing no evidence for other clouds in front of the Taurus cloud. Given that all of the late-type stars, plus the two early-type stars HD 29647 and 283809, have ice absorption features in their spectra, it seems reasonable to assume that this group must lie at or beyond the cloud distance of 140 pc. With normal reddening, however, two stars are too bright to lie at a distance of 140 pc. Elias 16, the most heavily reddened star in our sample, is too bright at K. Since the spectral type assigned to Elias 16 seems secure, and it is definitely not in front of the cloud, it seems that the assumption of normal extinction must be wrong. We find that $A_K \leq 0.27E(J-K)$ is necessary if Elias 16 is to lie at or beyond the cloud distance of 140 pc. Similarly, with normal reddening, HD 29647 is too bright at V to lie at 140 pc. For it to lie at or beyond this distance, $A_V \leq 5.4E(J-K)$ is necessary.

Assuming that most of the extinction for these two stars arises in the Taurus cloud, both of these results imply that the extinction law in the cloud is not a normal one. In fact, the

results suggest that $R \sim 3.5$–3.7 (e.g. Johnson 1968), as was already indicated by the HD 29647 and 283809 observations. On this basis, we assumed the above results to be valid for all of the stars that have detectable H_2O ice absorption, and proceeded to calculate A_V for each one using $A_V = 5.4E(J-K)$. These A_V values are listed in Table 1. The necessary $E(J-K)$ colour excesses were calculated using intrinsic $(J-K)$ colours from Frogel et al. (1978) for the late-type stars and from Whittet & van Breda (1980) for the early-type stars. We note that modest changes in R will not appreciably change our conclusions, so the assumption of a uniform (although abnormal) reddening law is not unreasonable.

3.3 Photospheric OH and the 2.96-μm feature

The scatter in the data points for the low-A_V late-type stars in Fig. 2(a) is in fact real structure which can be attributed to photospheric OH lines intrinsic to K and M stars. This is best illustrated in Fig. 3, where the spectrum of Tamura 17 is compared with the spectra of three late-type field stars, V842 Aql (M6III), HD 107003 (M2III) and BS 1286 (K1III). The data for V842 Aql were provided by Pendleton et al. (in preparation), while HD 107003 and BS 1286 were observed by us at the same time as the Taurus objects. Underneath the V842 Aql spectrum is displayed a grid which shows the positions of the strongest photospheric OH lines identified by Beer et al. (1972) in a high-resolution (FTS) spectrum of the M2Iab star α Ori (after smoothing to match our resolution). Fig. 3 shows quite clearly the development of OH features in the later spectral types, and shows that most of these lines are also pesent in the Tamura 17 spectrum. Also shown in Fig. 3 are the positions of three features resulting from H I absorption lines in the early-type standard star.

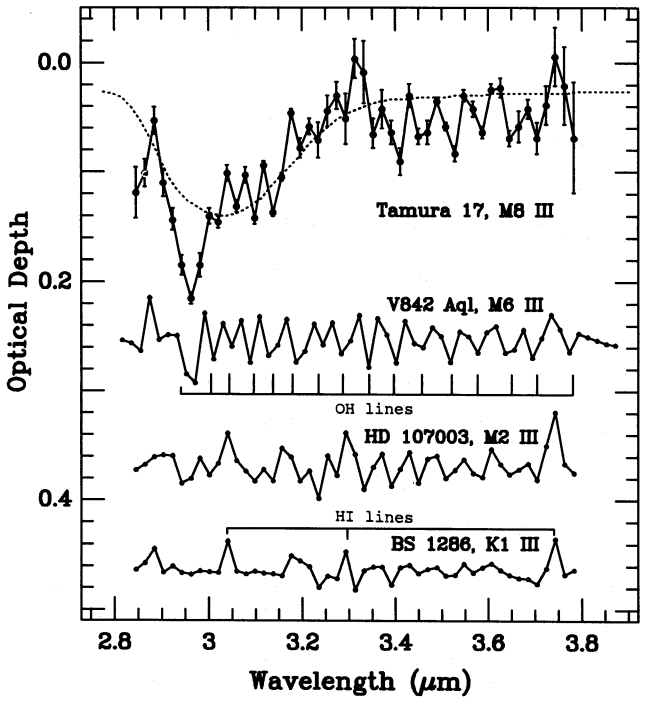

Figure 3. A comparison of the Tamura 17 spectrum, on an optical depth scale (error bars are $\pm 1\sigma$), with the spectra of three late-type stars from the general field (not behind the Taurus cloud), to illustrate which features in the Taurus spectra are photospheric in origin. The positions of the strongest photospheric OH absorption features are indicated under the V842 Aql spectrum (Pendleton et al., in preparation). On the K1III spectrum, the positions of features resulting from H I absorption in the standard star are marked. To facilitate comparison, the late-type stars have had a sloping baseline removed by dividing by a heavily smoothed version of themselves.

Apart from the 3.1-μm H_2O ice absorption, the dominant feature in the Tamura 17 spectrum is an absorption feature with a peak wavelength near 2.96 μm. In fact, an inspection of Fig. 2(a) reveals weak features near 2.96 μm in the spectra of several other stars in the sample. Interestingly, this wavelength is almost coincident with the wavelength of the fundamental N–H stretching vibration in NH_3 ice (2.963 μm: d'Hendecourt & Allamandola 1986). This led Graham & Chen (1991) to identify a feature near this wavelength in the spectra of the exciting stars of several Herbig–Haro objects with NH_3 ice. However, no absorption near this wavelength is seen in the spectra of any of the Taurus *early*-type stars in Fig. 2(b). In fact, an examination of the 'excess' absorption at 2.96 μm, i.e. after subtraction of the best-fitting H_2O ice-coated grain model (Section 4), suggests that the 2.96-μm feature is only significant in spectral types later than about K4III. This leads us to conclude that it is most probably a photospheric feature which develops in late-type stars. This conclusion is supported by the spectra in Fig. 3: a feature near 2.96 μm is absent from the K1III spectrum, it appears weakly in the M2III spectrum, and is the strongest feature in the M6III spectrum.

Although there are many photospheric OH features in these spectra, we cannot definitely identify the 2.96-μm feature with photospheric OH. It seems clear, however, that it is photospheric (or perhaps circumstellar) in origin, rather than arising in material in the Taurus cloud.

Tanaka et al. (1990) also see an absorption feature near 2.96 μm in the spectra of six M giants which lie behind the Ophiuchus dark cloud. Although they attribute this feature to absorption in circumstellar material because of its resemblance to a feature in the M9.0–M10.5 Mira NML Tau (observed by Scargle & Strecker 1979), it could just as easily be photospheric in origin. Again, the evidence points to an origin for the 2.96-μm feature in material local to the stars.

3.4 A_V versus $\tau_{3.05}$ and $\tau_{3.45}$

Figs 4(a) and (b) show plots of $\tau_{3.05}$ and $\tau_{3.45}$ against A_V, illustrating that a very good linear correlation exists in each case. The best linear least-squares fits to the data points are shown by the solid lines in each figure. The fits are, however, based on only those objects for which some H_2O ice absorption is measurable in the spectra. Representing the fits in the form $\tau_\lambda = m_\lambda(A_V - A_{V_0})$, following Whittet et al. (1988), where m_λ is the gradient and A_{V_0} is the threshold extinction for $\tau_\lambda = 0$, the following relations are obtained:

$$\tau_{3.05} = 0.059_{\pm 0.003}(A_V - 2.6_{\pm 0.6}) \quad \text{for } A_V > A_{V_0}, \qquad (1)$$

$$\tau_{3.45} = 0.0077_{\pm 0.0005}(A_V - 2.6_{\pm 0.8}) \quad \text{for } A_V > A_{V_0}. \qquad (2)$$

The threshold found for H_2O ice, $A_{V_0} = 2.6 \pm 0.6$, differs from the value of 3.3 ± 0.1 found by Whittet et al. (1988). This is consistent, however, with the differences between our estimates of A_V and the ice band optical depths and those of Whittet et al. The most interesting result must, however, be

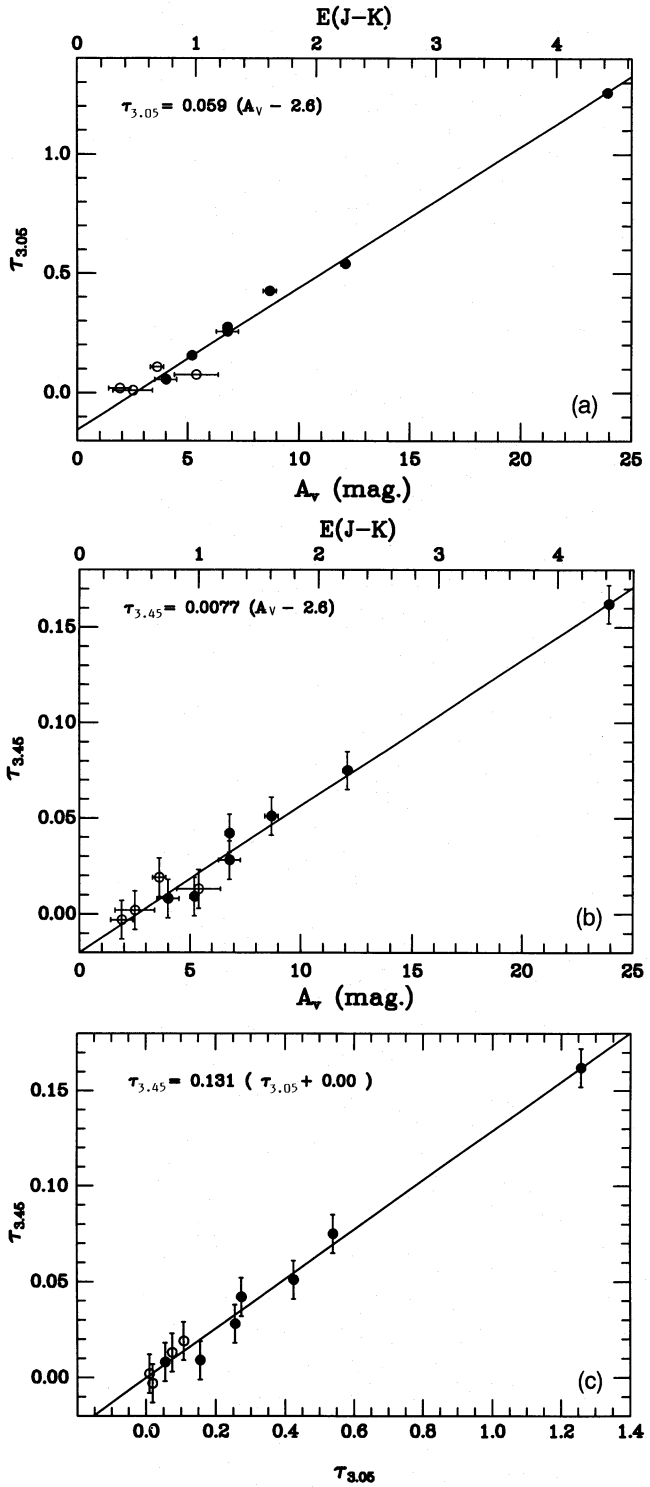

Figure 4. (a) The H_2O ice band optical depth, $\tau_{3.05}$, plotted against A_V (error bars are $\pm 1\sigma$ in all parts of this figure). The solid line shows the best linear fit to those data points for which $\tau_{3.05} > 0$. Filled and open circles represent the late-type and early-type stars, respectively, in the sample. (b) The optical depth in the long-wavelength wing, $\tau_{3.45}$, plotted against A_V. Here, $\tau_{3.45}$ is the observed optical depth *not* corrected for the H_2O ice contribution at 3.45 μm. The solid line shows the best linear fit to those data points for which $\tau_{3.45} > 0$. Symbols as in (a). (c) The strength of the long-wavelength wing, $\tau_{3.45}$, plotted against the strength of the H_2O ice band, $\tau_{3.05}$. Here, $\tau_{3.45}$ is the observed optical depth *not* corrected for the H_2O ice contribution at 3.45 μm. The solid line shows the best linear fit to the data points. Symbols as in (a).

the fact that, within the uncertainties, the H_2O ice band and long-wavelength wing have the same threshold extinction.

In Fig. 4(c), $\tau_{3.45}$ is shown plotted against $\tau_{3.05}$, and the best linear fit to the data points is given by the equation

$$\tau_{3.45} = 0.131_{\pm 0.006}(\tau_{3.05} + 0.00_{\pm 0.02}), \qquad (3)$$

where the zero intercept is a reiteration of the previous point, that the ice band and long-wavelength wing have the same threshold extinction.

Finally, we note that Tanaka et al. (1990) find a slope of 0.06 ± 0.01 for τ_{ice}/A_V in the Ophiuchus dark cloud, which is very close to the value we find for Taurus. Although Tanaka et al. find a very different threshold extinction for H_2O ice, $A_{V_0} = 10$–15, the fact that, within the uncertainties, the ratios of τ_{ice} to A_V are the same for both Taurus and Ophiuchus is an interesting result, suggesting that the physical conditions that govern mantle growth in Taurus may be common to many dark clouds.

4 THE GRAIN MODEL: CONSTRAINTS ON THE MANTLE THICKNESS

4.1 The basic grain model

In an attempt to constrain both the ice mantle thickness and the distribution of ice mantles in Taurus, we have developed an ice-coated grain model, based on Mie theory calculations for a mixture of small spherical graphite and silicate grains, coated with a layer of amorphous H_2O ice. In the model, the cores comprise nearly equal numbers of silicate and graphite grains, and are assumed to follow a power-law size distribution like that developed by Mathis, Rumpl & Nordsieck (1977, hereafter MRN). In this distribution the number density of grains with radii in the range a, $a + da$ is given by

$$n(a)\,da = An_H a^{-3.5}da, \qquad a_{min} < a < a_{max}, \qquad (4)$$

where the core radius, a, ranges from $a_{min} = 0.005$ μm to $a_{max} = 0.25$ μm, n_H is the number density of hydrogen atoms, and A is a constant, which is different for each component. For the graphite component, $A_{(Gr)} = 10^{-25.16}$ cm$^{2.5}$ H^{-1}, while, for the silicates, $A_{(Si)} = 10^{-25.11}$ cm$^{2.5}$ H^{-1}. These constants are values found by Draine & Lee (1984) to give the best fit to the average interstellar extinction curve. The basic MRN distribution was chosen because it has been found to give results consistent with measurements of the extinction and polarization in both the visible and the UV, and out into the infrared (Draine & Lee 1984). We have initially assumed that all of the grains receive the same H_2O ice mantle thickness (*not* volume), which is physically realistic if the sticking coefficient of a molecule on to the grain surface is independent of the grain size (Draine 1985a). Optical constants for the mantle are those of 23-K amorphous H_2O ice, from Kitta & Krätschmer (1983), while the optical constants for the cores have been taken from the tabulated optical properties of 'astronomical silicate' and graphite by Draine (1985b). The choice of 23 K for the ice temperature reflects the limited availability of ice optical constants. There is no significant difference, however, between these and the 10-K optical constants of Hagen, Tielens & Greenberg (1981) (except that the latter cover a smaller wavelength range), so we are essentially modelling cold (10–20 K), amorphous H_2O ice.

The model provides an extinction optical depth at a wavelength λ of

$$\tau_\lambda = n_{\rm H}\left[\int_{a_{\rm min}}^{a_{\rm max}} A_{\rm (Gr)} a_{\rm core}^{-3.5} C_{{\rm Gr},\lambda}(a_{\rm core}+a_{\rm th})\,{\rm d}a + \int_{a_{\rm min}}^{a_{\rm max}} A_{\rm (Si)} a_{\rm core}^{-3.5} C_{{\rm Si},\lambda}(a_{\rm core}+a_{\rm th})\,{\rm d}a\right], \quad (5)$$

where $C_{{\rm Gr},\lambda}(a_{\rm core}+a_{\rm th})$ and $C_{{\rm Si},\lambda}(a_{\rm core}+a_{\rm th})$ are the extinction cross-sections for an MRN distribution of ice-coated spherical graphite and silicate grains of radius $a_{\rm total}(=a_{\rm core}+a_{\rm th})$. In this simplest form of the model there are only two variables, the total hydrogen column density and the H_2O ice mantle thickness $a_{\rm th}(=a_{\rm total}-a_{\rm core})$.

Although we have tried to be as realistic as possible in terms of grain size distribution and grain composition, we have found it necessary to treat the grains as spherical core-mantle particles for our calculations. The extinction resulting from different grain shapes such as cylinders, spheroids and fractal grains has previously been investigated (e.g. van de Bult, Greenberg & Whittet 1985; Draine 1985b; Mathis & Whiffen 1989; Bazell & Dwek 1990), but none of these papers has considered the additional complication of adding an ice mantle to a non-spherical grain core. Such a calculation is, however, well beyond the scope of this paper.

4.2 Observational constraints

There are a number of constraints that arise from the observations, which must be taken into account in the modelling.

(1) The good correlation between $\tau_{3.05}$ and A_V (Fig. 4a and Section 3.4) means that $\tau_{3.05}/A_V = 0.059(\pm 0.003)$ must hold true for most of the sample. The model can be used to compute this ratio, from $\tau_{3.05}/\tau_V$, although it is important to note that the observed value of $\tau_{3.05}$ (i.e. as listed in Table 1) is not the *total* extinction at 3.05 μm, but is the extinction resulting only from H_2O ice, because we have reddened a stellar continuum to fit the observations, and have determined $\tau_{3.05}$ relative to this continuum, thereby eliminating the component of the extinction resulting from the dust grains themselves. Thus the *model* value of $\tau_{3.05}$ has been determined by subtracting the underlying dust extinction, obtained by interpolating between points on either side of the ice band.

(2) The observed R-values of several of the Taurus stars range from 2.8 to 3.5 (Section 3.2). We can ensure that the model yields an R-value that is physically reasonable by computing R from $\tau_V/(\tau_B-\tau_V)$ $[\equiv A_V/E(B-V)]$. However, as Mathis & Wallenhorst (1981) point out, the R-value calculated for an MRN distribution is quite sensitive to the choice of optical constants and to the exact wavelengths assigned to B and V, so we do not require an exact match to the observed R-value, but instead use the computed R-value only as an indication of when the model goes beyond reasonable bounds.

(3) A fundamental constraint is obtained by calculating the percentage of oxygen tied up in H_2O in the mantles. The H_2O ice mantle volume from the models yields directly the number of oxygen atoms on the grains. The actual amount of oxygen available can be obtained by first computing the H-atom abundance by taking the grain volume per H atom in the MRN size distribution to be 5.7×10^{-27} cm^3 H^{-1} (Draine 1985a), and then assuming a cosmic abundance of oxygen. This can be compared with the estimated 10 per cent oxygen depletion in Taurus (in the form of H_2O ice) calculated by Whittet (1992) using the laboratory-determined value of the integrated absorbance (cm molecule^{-1}) of H_2O ice in conjunction with the observed ice band optical depth.

(4) The final but perhaps most obvious constraint is that the model must be able to provide a reasonable fit to the observed ice band profile.

In Fig. 5(a) the computed $\tau_{3.05}/A_V$ ratios and R-values are plotted against mantle thickness for the model described above, and Table 2 summarizes the results obtained for several relevant mantle thicknesses. The bare MRN model, i.e. without ice mantles (by default model 1), provides a point of reference and, although the value of $R=3.3$ produced by this model is slightly different from the normally accepted value of 3.1, it is still close enough to allow us to judge whether large excursions from the norm occur when ice mantles are added. Model 2 was chosen to yield a correct value of $\tau_{3.05}/A_V$, model 3 serves as an upper limit because it uses 100 per cent of the available oxygen (in the form of H_2O ice), and model 4 is the result of an unconstrained fit to find the model which best matches the observed ice band profile (note that a conservative estimate of the uncertainty in the model 4 fit is $a_{\rm th}=0.35\pm0.05$ μm). In Fig. 5(b), models 2, 3 and 4 have been fitted to the Elias 13 spectrum (with the assumption that Elias 13 is reasonably representative of the entire sample).

Unfortunately, none of these models satisfies all of the observational criteria. Clearly, the two with the thinnest mantles (models 2 and 3) provide a very poor fit to the observed ice band profile, but there is a serious problem with the model that does fit (model 4), in that it uses far more than the available abundance of oxygen. It also yields a value for the ratio $\tau_{3.05}/A_V$ which is much larger than the observed value of 0.059 (see Table 2).

Accepting that the thick mantles of model 4 are necessary to fit the observed ice band profile, we need to find a way to modify this model to satisfy the other observational constraints. The abundance constraint and the large $\tau_{0.35}/A_V$ value argue that the amount of ice in the mantles (i.e. $\tau_{3.05}$) in model 4 must be reduced, although simple reduction of the mantle thickness is not a solution because this degrades the previously good match to the observed H_2O ice band shape (Fig. 5b). Alternatively, the grain core extinction (i.e. A_V) needs to be increased while still retaining thick ice mantles on the grains. Three possible solutions are that (i) the grain (core) size distribution is incorrect, (ii) the assumption of a constant mantle thickness is incorrect, or (iii) some of the grains have no ice mantles.

4.2.1 *Alternative grain (core) size distributions*

There is no guarantee that the MRN grain model is applicable in dark clouds where, for example, coagulation could alter the grain size distribution. In fact, there is considerable evidence for grain growth or at least a modification of the grain size distribution in dense clouds, in the form of substantially different R-values in many lines of sight. To what

extent this might depend on the accretion of molecular mantles, rather than on coagulation, is, however, not clear.

Taking the MRN model as our basis, we have explored the effects of modifying the upper and lower limits to the grain (core) size distribution, assuming that some coagulation might have taken place in the dark cloud environment (but still retaining the constant-thickness ice mantles). To limit the range of parameters to be examined, the power-law index has been held fixed at the MRN value of -3.5 and the total grain core volume has been constrained to match the original MRN volume. This may be an oversimplification of the coagulation effects, which might result in a power-law index other than -3.5, but, if the MRN distribution is assumed to be valid in the diffuse ISM and at the edges of the Taurus cloud, this is a reasonable 'first guess' at the grain size distribution. In any event, a full examination of all possible grain size distributions is beyond the scope of this work.

Fig. 6(a) shows several plots of $\tau_{3.05}/A_V$ against mantle thickness, and Table 3 summarizes the model results for this modified grain size distribution, for those mantle thicknesses yielding a value of $\tau_{3.05}/A_V$ that matched the observed value. To illustrate how these fit the observations, Fig. 6(b) shows several fits to the Elias 13 spectrum. It is clear, from both the figures and the table, that none of the models yields an acceptable result. To provide more extinction at longer wavelengths (relative to shorter wavelengths) where the fit is worst,

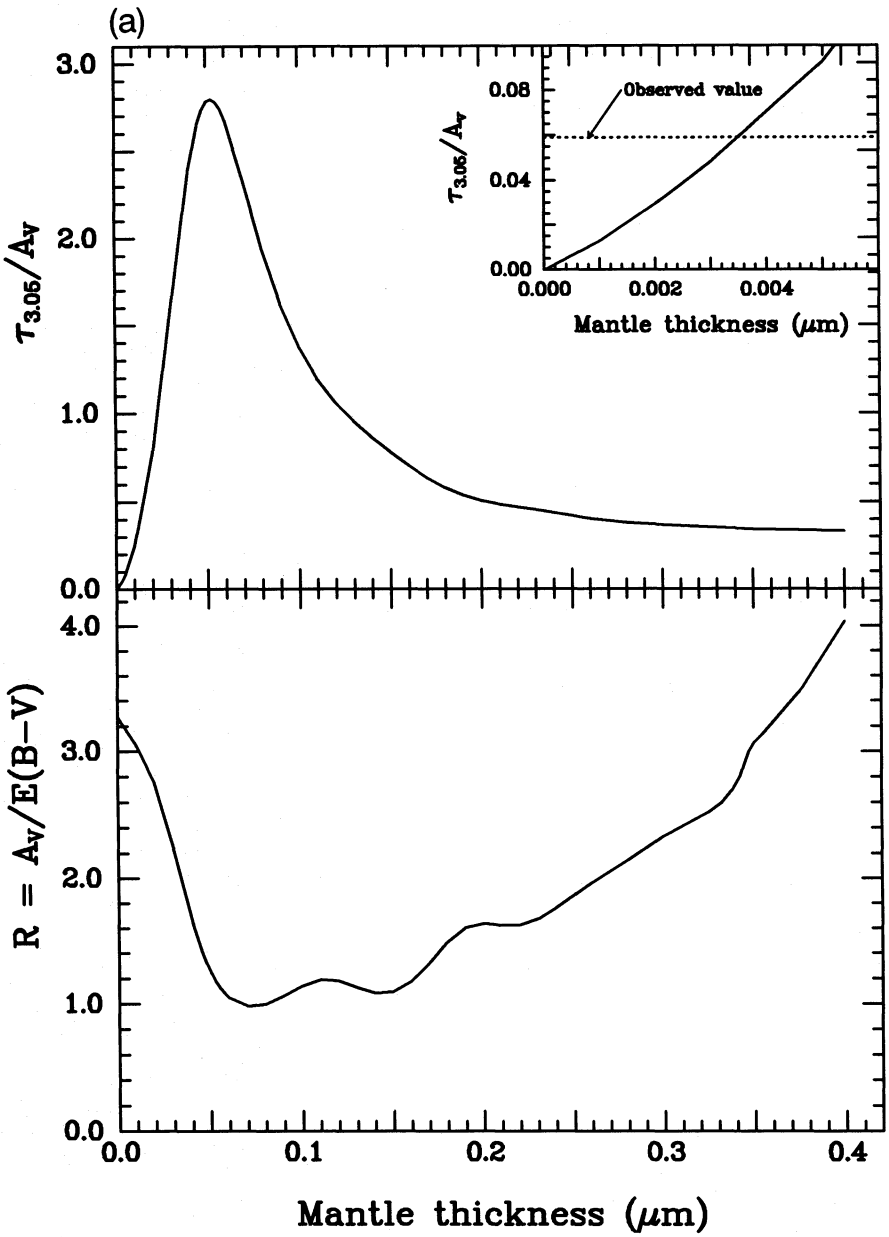

Figure 5. (a) Top panel: the calculated ratio $\tau_{3.05}/A_V$ plotted against mantle thickness for a model with an MRN core distribution and a constant mantle thickness. The inset is an enlargement of the region near the origin and shows where the model value of $\tau_{3.05}/A_V$ (0.059) coincides with the observations. Bottom panel: the variation in the calculated R-value with mantle thickness. (b) Results from H_2O ice-coated grain models (models 2, 3 and 4) fitted to the Elias 13 spectrum. The models have a constant mantle thickness on grains that are composed of silicate and graphite cores, and whose core radii follow an MRN size distribution.

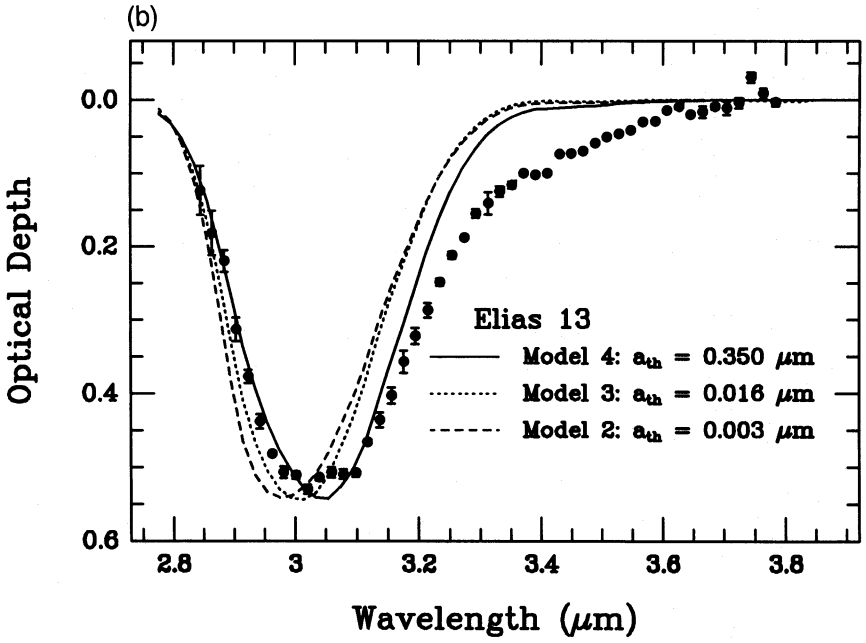

Figure 5 – *continued*

Table 2. Comparison of grain models: constant mantles and MRN cores.

Parameter	Bare MRN	Model 2	Model 3	Model 4
Cores:				
a_{min}	0.005 μm	0.005 μm	0.005 μm	0.005 μm
a_{max}	0.25 μm	0.25 μm	0.25 μm	0.25 μm
Mantles:				
a_{th}	0.0 μm	0.003 μm	0.016 μm	0.35 μm
R	3.3	3.2	2.9	3.1
$\tau_{3.05}/A_V$	0.0	0.059	0.538	0.342
Oxygen depletion	0%	9%	100%	54400%

an increase of the average grain size is needed (i.e. as the grain size is increased, scattering makes a larger contribution to the extinction near 3.1–3.2 μm). Judging by the calculated R-value (Table 3), however, even modest increases in the average grain size are unacceptable. Thus a larger than normal MRN size distribution, modified as outlined above, cannot explain the Taurus observations.

4.2.2 *A variable mantle size distribution*

The accretion of molecular mantles can also change the grain size distribution, and we already know that there are icy grain mantles in Taurus, so it need not be the grain core size distribution that changes. Let us now assume that the MRN model best describes the size distribution of the grain cores throughout Taurus. Numerically, the small grains dominate the MRN distribution, which means that, for a model with constant mantle thickness, most of the ice will be on the smaller grains. The only way to reduce the amount of ice on the grains to comply with the abundance constraints, while still retaining some large H_2O ice-coated grains to provide a good match to the ice band profile, is to reduce the thickness of the mantles on the smaller grains.

To examine this possibility, the model has been modified so that the mantle thickness, a_{th}, follows a power-law distribution, i.e.

$$a_{th} = \text{constant} \times a^{\beta}, \tag{6}$$

where a is the core radius, and the index β is a free parameter. Fig. 7(a) shows how the ratio $\tau_{3.05}/A_V$ depends upon maximum mantle thickness for this model, for several values of the index β, and Table 4 summarizes the model results for those mantle distributions yielding a value of $\tau_{3.05}/A_V$ that matched the observed value. Several of these models are also shown fitted to the Elias 13 spectrum in Fig. 7(b).

The best-fitting model is clearly model 14. This model also satisfies all of the observational constraints. It must, as a matter of course, match the observed $\tau_{3.05}/A_V$ ratio, since this was part of the acceptance criteria. However, the model also yields an R-value of 3.7, which is consistent with the higher than normal value found for the two early-type stars that have ice mantles (i.e. $R = 3.5$; see Section 3.2). The oxygen depletion resulting from H_2O ice in the grain mantles in model 14 is also reasonable, at ~ 8 per cent.

To see what this model means in terms of the distribution of ice mantles, in Fig. 8 the mantle thickness is plotted against grain radius for a number of values of the index β, from equation (6). This shows, from the best-fitting ($\beta = 11$) curve, that most of the ice is on the large grains. Some measure of the uncertainty in the power-law index is given by the fact that, in the process of fitting this model to the entire sample, we find that the best fits are achieved for indices in the range $\beta = 7$–11. However, this could simply be attributed to small local variations in the grain mantle thicknesses. Reasonable fits can also be achieved with a smaller index, but

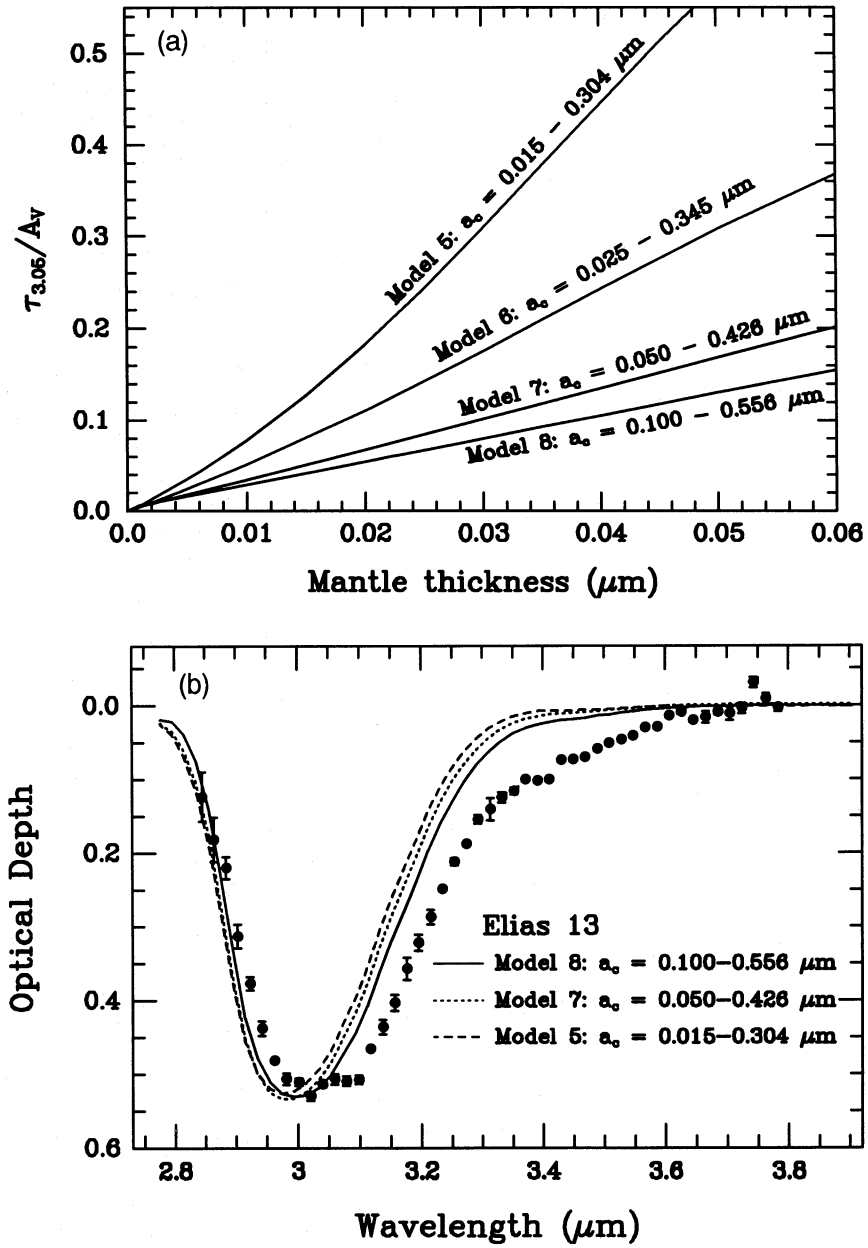

Figure 6. (a) The calculated ratio $\tau_{3.05}/A_V$ plotted against mantle thickness for a model which has a larger than normal MRN core distribution and a constant mantle thickness. The lines are labelled with the minimum and maximum values of the core radii used in this model, and results from models 5, 6, 7 and 8 are shown. (b) Results from H_2O ice-coated grain models (models 5, 7 and 8) fitted to the Elias 13 spectrum. The models have a constant mantle thickness on grains that are composed of silicate and graphite particles, and that follow a larger than normal MRN size distribution (i.e. the upper and lower limits of the MRN distribution are increased beyond their normal values; see text).

only if the upper limit on the grain (core) size distribution is increased beyond 0.25 μm.

4.2.3 A mixture of 'bare' and 'mantled' grains

An alternative to having ice mantles only on the largest grains is to have a constant ice mantle thickness on all grains, independent of grain size, but also to consider that there are two grain populations, one of bare and one of ice-coated grains. This has the desired effect of increasing A_V relative to $\tau_{3.05}$ and lowering the oxygen depletion, while still maintaining the thick mantles necessary to fit the observed ice band profile. However, the constancy of the $\tau_{3.05}/A_V$ ratio, which is observed to remain the same throughout the cloud, is maintained *only* if the optical depth of the bare and mantled regions in the cloud vary together. Simple addition of a region of bare grains of fixed optical depth, for example in front of the cloud, would only shift the zero-point of the $\tau_{3.05}$ versus A_V relation in Fig. 4(a) – it would not change the slope. Similarly, addition of a region of bare grains in the middle of the cloud would increase A_V for all stars observed through this material, but still would not change the $\tau_{3.05}/A_V$ relation for these stars. From our models, we calculate that the visual extinction cross-section of an MRN grain distribu-

Table 3. Comparison of grain models: constant mantles and large MRN cores.

Parameter	Model 5	Model 6	Model 7	Model 8
Cores:				
a_{min}	0.015 μm	0.025 μm	0.050 μm	0.100 μm
a_{max}	0.304 μm	0.345 μm	0.426 μm	0.556 μm
Mantles:				
a_{th}	0.008 μm	0.011 μm	0.017 μm	0.022 μm
R	3.8	4.3	6.4	22.4
$\tau_{3.05}/A_V$	0.059	0.059	0.059	0.059
Oxygen depletion	11%	10%	10%	8%

tion with 0.35-μm ice mantles is a factor of $\sim 7\times10^3$ larger than that of a 'bare' MRN distribution. Some physical insight into this factor is gained by noting that it roughly corresponds to the ratio of the total grain volumes in the two distributions. If we then solve the simple equation (using optical depths from models 1 and 4)

$$\frac{\tau_{3.05(\text{model 4})}}{1.086\,[\tau_{V(\text{model 4})}+n_b\,\tau_{V(\text{bare MRN})}]}\sim\frac{\tau_{3.05(\text{obs})}}{A_{V(\text{obs})}}=0.059 \qquad (7)$$

for n_b, the ratio of the numbers of bare and ice-coated grains, we find that of the order of 3×10^4 bare grains would be required for every ice-coated grain to reproduce the observed $\tau_{3.05}/A_V$ ratio of 0.059 (note that this assumes that all of the ice-coated grains have 0.35 μm thick mantles).

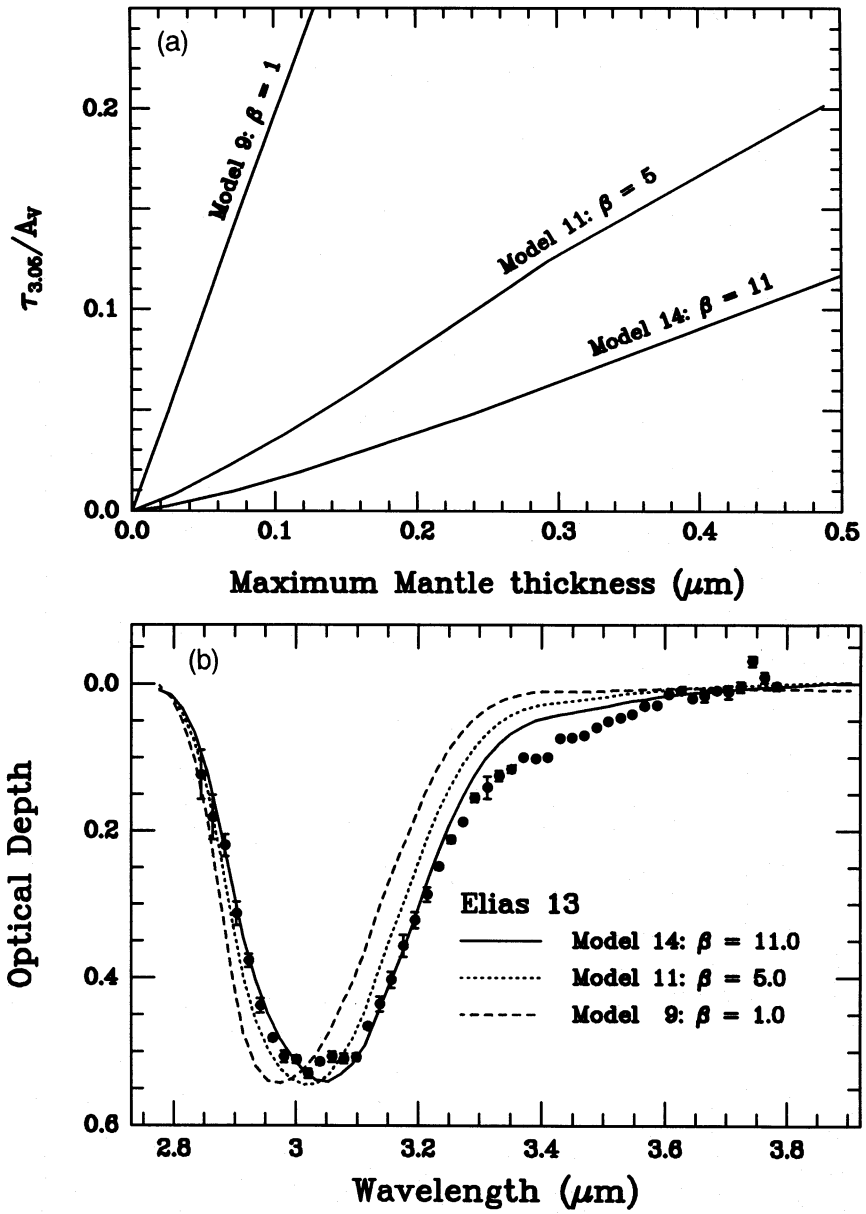

Figure 7. (a) The calculated ratio $\tau_{3.05}/A_V$ plotted against maximum mantle thickness for models that have an MRN core distribution and a variable mantle thickness (i.e. one that follows a power law, index β). Results from models 9, 11 and 14 are plotted. (b) Results from H_2O ice-coated grain models (models 9, 11 and 14) fitted to the Elias 13 spectrum. The models have a mantle thickness that depends on the core radius a as a^β (indices indicated on the key) on silicate and graphite cores whose core radii follow an MRN size distribution.

Table 4. Comparison of grain models: variable mantles and MRN cores.

Parameter	Model 9	Model 10	Model 11	Model 12	Model 13	Model 14
Cores:						
a_{min}	0.005 μm	0.005 μm	0.005 μm	0.005 μm	0.005 μm	0.005 μm
a_{max}	0.250 μm	0.250 μm	0.250 μm	0.250 μm	0.250 μm	0.250 μm
Mantles:						
Constant	0.12	6.5	158	3.3×10^3	6.4×10^4	1.2×10^6
Index, β	1.0	3.0	5.0	7.0	9.0	11.0
Maximum mantle thickness	0.030 μm	0.102 μm	0.154 μm	0.201 μm	0.244 μm	0.281 μm
R	3.4	3.9	3.9	3.8	3.7	3.7
$\tau_{3.05}/A_V$	0.059	0.059	0.059	0.059	0.059	0.059
Oxygen depletion	10%	8%	8%	8%	8%	8%

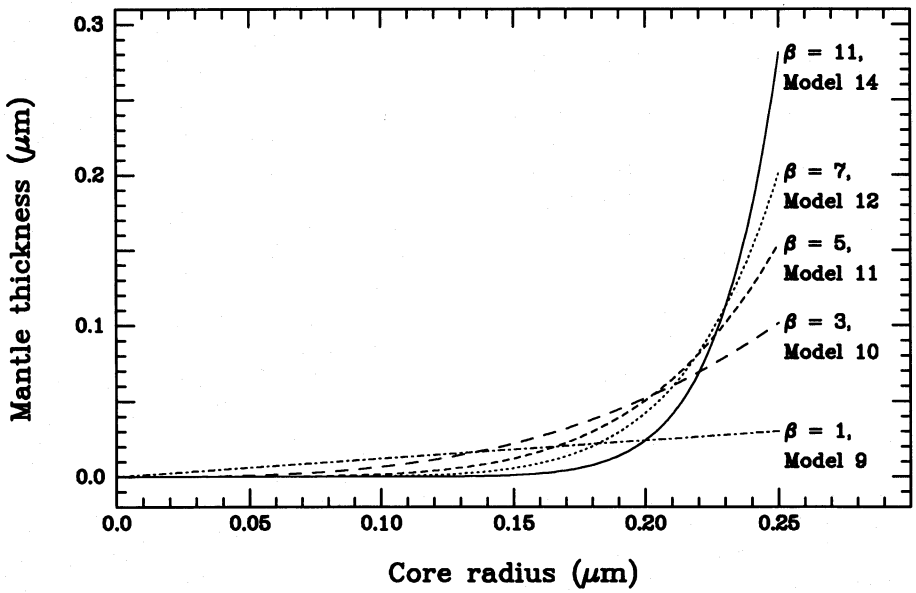

Figure 8. An illustration of the distribution of H_2O ice mantles on the grains in the models that have an MRN core size distribution and mantles that follow a power-law distribution. Models 9, 10, 11, 12 and 14 are plotted ($\beta = 1, 3, 5, 7$ and 11 respectively).

Calculating the oxygen depletion, we find that ~9 per cent of the available oxygen, in the form of H_2O ice, is tied up in the grain mantles, in excellent agreement with the depletion estimate of Whittet (1992). In fact, looking over the model results above, we see that the oxygen depletion is almost independent of the choice of model since *all* models satisfying $\tau_{3.05}/A_V = 0.059$ yield an oxygen depletion in the range 8–11 per cent. This presumably reflects a relationship between the $\tau_{3.05}/A_V$ ratio and the ratio of the H_2O ice volume to the grain (core) volume, because all of the models must reproduce the observed value of this ratio (0.059) to be accepted.

We calculate R [$= A_V/E(B-V)$] for the bare/ice-coated grain combination to be ~3.3. This is slightly lower than the value of $R = 3.5$ observed for two early-type stars in our sample (Section 3.2), but still acceptable given the uncertainties in the calculation of an R-value from the model. In fact, R is strongly dependent on the mantle thickness [Fig. 5(a)], so a relatively modest increase in a_{th} from 0.35 μm could significantly increase the calculated R-value. Alternatively, only a small modification of the grain core size distribution (e..g. through coagulation) would be required to raise R to the observed value. The significant implication from this model is that the majority of the grains have no H_2O ice mantles.

In summary, two types of model yield reasonable oxygen depletions and R-values, and provide reasonable fits to the observed ice band profile. One model (model 14; Figs 7a and b), in which the ice mantle thickness increases with grain size, requires that only the largest grains have significant ice mantles. The other model requires that only a small fraction of the total grain population has any mantle at all, but those grains that do have ice mantles of constant thickness (model 4; Figs 5a and b).

5 DISCUSSION

5.1 The H_2O ice threshold

One mechanism for production of the observed H_2O ice threshold of $A_{V_0} \sim 2.6$ is *simple thermal evaporation* from grains near the edges of the cloud, which are heated by external UV. However, we should then be able to associate this threshold with the condensation temperature of H_2O. This would mean that grains at this threshold should have temperatures of ≥ 100 K (e.g. Nakagawa 1980), but such a high temperature is very difficult to reconcile with the dust temperature of 18–26 K determined for Taurus from *IRAS* 60- and 100-μm data by Snell, Heyer & Schloerb (1989). This temperature estimate is consistent with the grain temperatures of 12–20 K calculated by Draine & Lee (1984) for graphite and silicate grains exposed to an 'average' interstellar radiation field (for grain radii of between 1.0 and 0.01 μm). The net result is that we do not expect to find grain temperatures in excess of ~26 K in the Taurus dark cloud, so simple thermal evaporation of H_2O from grain surfaces should not be important.

This view is supported by the Taurus observations themselves, because there is no evidence for annealing of the H_2O ice. In the laboratory, the width of the 3.1-μm H_2O ice absorption decreases as the temperature is increased (Hagen et al. 1981), so, if the grain temperatures reach anywhere near 100 K, we would expect to see some indication of this in the form of a change in the observed width of the H_2O ice feature. The work of Smith et al. (1989) illustrates different observed H_2O ice band profiles, corresponding to a range of ice temperatures. Elias 16, in particular, has a broader profile than do many of the other sources, indicative of lower temperatures. However, all of the Taurus field stars show a similar ice band profile, within the uncertainties (Figs 2a and b).

There are other desorption mechanisms, which involve *thermal spikes* produced when the grain absorbs a UV or visible photon or cosmic ray. This process should be most effective for small grains near the edges of the cloud (see e.g. Watson & Salpeter 1972a; Draine & Salpeter 1979). However, Draine (1985a) argues that UV or visible photons cannot prevent H_2O from accreting on grains larger than ~20 Å, while 'typical' cosmic rays cannot prevent H_2O from accreting on grains larger than ~10 Å. Thus thermal spikes should be ineffective for the bulk of the MRN grain distribution.

The simplest mechanism to explain the absence of H_2O ice mantles at the cloud edges in Taurus appears to be *photodesorption*, where the photon energy goes into breaking individual molecular bonds rather than heating the grains (see e.g. Draine & Salpeter 1979; Boland & de Jong 1982). Although the photodesorption efficiency is somewhat uncertain, we can obtain a lower limit to the photodesorption rate per adsorbed molecule using a simplified form of an expression from Boland & de Jong (1982),

$$r_{pd} \sim 10^{-12} \exp(-1.84 A_V) \quad s^{-1}, \tag{8}$$

and compare it with the accretion rate for oxygen atoms per surface site, also simplified, from Wickramasinghe (1967; see also Draine & Salpeter 1979),

$$r_{acc} \sim 3 \times 10^{-16} n_H T_{gas}^{1/2} \quad s^{-1}, \tag{9}$$

which suggests that photodesorption could nominally keep a grain bare of H_2O ice mantles for $A_V < 1$ in a moderate-density cloud ($n_H = 100$ cm^{-3}) if a gas kinetic temperature of $T_{gas} = 50$ K (Watson & Salpeter 1972b) is adopted. However, a more realistic scenario is one in which external UV radiation can at least affect dust at the front and back of the cloud in any (arbitrary) line of sight through Taurus, which immediately raises the above threshold to $A_V < 2$. The desorption rate need not be very much higher to explain the observed H_2O ice threshold at $A_V \sim 2.6$. In fact, if the cloud structure is irregular or 'clumpy' (see Section 5.2), external UV may be able to penetrate into the interior regions of the cloud, thereby raising the threshold A_V. Given the uncertain efficiency of this process, this is a reasonable result, and photodesorption seems to be the most promising desorption mechanism to explain the H_2O ice threshold.

An alternative mechanism has been proposed by Williams, Hartquist & Whittet (1992). Some clouds have a much higher H_2O ice threshold than Taurus, requiring a significant enhancement of the UV field. Ophiuchus, for example, has $A_{V_0} = 10$–15 (Tanaka et al. 1990). Williams et al. have proposed that the absorption of *infrared* photons near the peak of the H_2O ice feature at 3 μm could lead to the ejection of physisorbed H_2O molecules from grain surfaces, providing an additional means of preventing the accumulation of ice mantles. The efficiency of this process compared to other desorption mechanisms is, however, not clear. The presence of significant star formation in Ophiuchus, for example, suggests an enhanced local UV field and a corresponding increase in the UV photodesorption rate, which could also be augmented if the cloud structure is such that external and local UV radiation can penetrate deeply into the cloud.

We note that these arguments may not necessarily apply to CO ice, which has a threshold extinction of ~5.3 in Taurus (Whittet et al. 1989), substantially different from that of H_2O ice (= 2.6). However, CO has a condensation temperature in the range 17–24 K (Nakagawa 1980; Sandford & Allamandola 1988), close to the nominal grain temperature, so simple thermal evaporation or thermal spikes could very well be responsible for preventing CO from accumulating on grains near the edges of the cloud. In fact, Léger, Jura & Omont (1985) argue that, for CO rich mantles, even whole-grain heating (by either UV photons or cosmic rays) should be efficient at desorbing CO over the entire size range of the MRN distribution, up to $A_V \sim 5$.

5.2 The size of the grain mantles in Taurus

The model results outlined in Section 4.2 indicate two possible scenarios for the grain mantles in Taurus: (1) there are two grain populations, one comprising a large fraction of the total population, bare of mantles, and the other having thick H_2O ice mantles; or (2) there are effectively no mantles on the smaller grains in the MRN distribution. It is also apparent that the $\tau_{3.05}/A_V$ ratio is relatively constant for the entire sample (Fig. 4a), which suggests that whatever mechanism determines the mantle size or fraction of ice-coated grains must be active throughout the cloud. We add to this the basic observation that the entire gas phase is clearly *not* depleted on to grains deep in the cloud, again indicating that some desorption mechanism must be active throughout most of the cloud.

Physically, scenario (2) could be interpreted as meaning that the sticking coefficient for molecules on to the grains is not independent of grain size. This could mean that additional factors play a role in determining whether molecules stick to grain surfaces. For example, there could be a mechanism acting in Taurus to remove molecules selectively from the small grains. Thermal spikes resulting from the absorption of UV or visible photons or cosmic rays could selectively desorb molecules from the surfaces of small grains, but as stated earlier the calculations of Draine (1985a) suggest that this would be ineffective for grains larger than ~ 20 Å. In addition, for UV or visible photons to affect the entire Taurus grain population, they must be able to penetrate deep into the cloud.

Another possibility, which also requires that some UV radiation be able to penetrate into the cloud interior, is that the UV radiation reaching the grains, while not sufficient to desorb molecules directly from the surface, could induce chemical explosions in the mantles. Greenberg (1973; see also d'Hendecourt et al. 1982) has proposed that exposure of molecular cloud ices to UV radiation can result in the production of chemical radicals in the ice. Because of the low temperatures these radicals do not react immediately, but provide a form of stored 'chemical energy' which can be released if the grain temperature is raised above a threshold of ~ 25 K, when the resulting chemical explosion can eject the entire mantle. One uncertainty about this process is whether grain temperatures in excess of 25 K are reasonably deep inside the cloud. Mantle explosions may, however, be a way to obtain a variable mantle thickness, since the explosions may not be as effective at removing the entire mantle from the larger grains.

Scenario (1), like the other mechanisms discussed above, also requires the penetration of external UV photons deep into the cloud, to explain the large numbers of bare grains. However, neither photodesorption nor any of the other desorption mechanisms discussed above appears to be able to affect mantles on grains in the cloud interior if the cloud has a uniform structure (Section 5.1; Draine & Salpeter 1979; Léger et al. 1985; Draine 1985a). To explain this problem, Boland & de Jong (1982) have suggested that turbulence could be effective at recycling gas and dust from the edges of the cloud throughout the cloud interior; the grains are subject to photodesorption when they come near the cloud edges.

An alternative explanation is that the density structure in Taurus is clumpy or filamentary (which may well be a consequence of turbulence), and the lower density regions between the clumps allow external radiation to penetrate deeper into the cloud. This scenario was originally proposed by Stutzki et al. (1988) to explain the [C II] emission in M17. While the efficiency of turbulent mixing is unknown, there is direct observational evidence for clumpy structure in Taurus (Ungerechts & Thaddeus 1987; Dickman, Horvath & Margulis 1990). Thus the large number of bare grains in scenario (1) could result from external radiation penetrating deep into the cloud between the clumps, with photodesorption preventing H_2O ice mantles from accumulating on the grains at the edges of these clumps. If only a small fraction of the grains in the cores of these clumps are able to condense ice mantles, this would also explain why the entire gas phase is not depleted on to the grains in the cloud interior. An additional implication is that the sizes of the clumps must be small compared with the lengths of the columns that we are sampling through the cloud, otherwise significant variations in the $\tau_{3.05}/A_V$ ratio ratio would be seen in different lines of sight. Dickman et al. (1990) found density fluctuations in Taurus on a scale of 0.3 pc or less. To compare this to our data would require selection of where the $\tau_{3.05}$ versus A_V relationship (Fig. 4a) starts to break down at low A_V. However, our data are not good enough to choose where or indeed whether this breakdown occurs, so we are not able to place any meaningful constraints on the clump size.

In summary, although the model results reveal two possible ways in which the ice mantles could be distributed on the grains in Taurus, there are sufficient uncertainties surrounding the variable-mantle-thickness scenario that we would argue in favour of the simplest scenario (and the one supported by the most observational evidence): the clumpy density structure of the Taurus cloud.

5.3 The origin of the long-wavelength wing

In this discussion, we consider only the three most common explanations for the long-wavelength wing.

5.3.1 Scattering by large ice-coated grains

The good fit of our models to the observed ice band profile in Figs 5(b) and 7(b) suggests that the inclusion of slightly larger grains might provide enough additional extinction near 3.4 μm to explain all of the absorption in this region. An examination of the 3-μm spectra of several protostars (Smith et al. 1989), however, reveals several sources with a great deal more absorption at 3.4 μm (relative to H_2O ice) than is seen in Taurus. Thus it is not simply a matter of invoking slightly larger grains to explain the long-wavelength wing: many grains of much larger sizes are required. After examining a wide range of models, we have not been able to find a grain size distribution that can provide this additional extinction and still satisfy all of the observational constraints.

5.3.2 $NH_3 \cdot H_2O$ mixtures

Mixtures of H_2O and NH_3 certainly produce additional absorption in the 3.4-μm region (see e.g. d'Hendecourt & Allamandola 1986), as a result of the formation of N···H–O bonds in the mixture (i.e. this moves the N–H stretch from 2.96 to ~ 3.44 μm). The major problem with this explanation is that, in moderate-resolution ($\lambda/\Delta\lambda \sim 640$) spectra of two protostars with strong ice bands and long-wavelength wings, Smith et al. (1989) failed to find any sign of the fundamental N–H stretching vibration of NH_3 near 2.96 μm. In the absence of any direct evidence for NH_3 molecules in grain mantles, the only way in which $NH_3 \cdot H_2O$ mixtures can be viable is if *all* of the NH_3 molecules form N···H–O bonds. However, this is not evident in the laboratory mixtures studied to date.

5.3.3 Hydrocarbons

The fundamental C–H stretching vibration falls in the 3.2–3.6 μm range, and there is substantial evidence for the existence of hydrocarbons as a component of the dust in

other phases of the ISM: in the diffuse ISM in the form of an absorption feature near 3.4 μm (Sandford et al. 1991), and in the form of a number of emission features in this wavelength range associated with dust in planetary nebulae, H II regions, young stellar objects, galaxies and comets (see e.g. Tokunaga & Brooke 1990). On the basis of available observations and laboratory work, we see two possible forms that hydrocarbons could take in the Taurus dust grains: (i) simple hydrocarbons (e.g. CH_4, CH_3OH, etc.) could be mixed with the H_2O and CO ices in the grain mantles; or (ii) a much more refractory hydrocarbon mixture, like that identified in the diffuse ISM (Sandford et al. 1991), or the polycyclic aromatic hydrocarbons (PAHs) or hydrogenated amorphous hydrocarbons (HACs) proposed as explanations for the IR emission features (see e.g. Sellgren 1990), could be present as an intrinsic part of the grains. Linking these two scenarios is the proposal by Greenberg (1982) that refractory hydrocarbon residues might be produced by the photolysis of 'typical' molecular cloud ices. Strong support for this proposal has been provided by the detection in the diffuse ISM of an absorption feature near 3.4 μm, which is well matched by the residues from laboratory photolysis of simple ice mixtures (e.g. Sandford et al. 1991).

Whichever scenario we consider requires the presence of hydrocarbons on the grains throughout the cloud, because the long-wavelength wing is seen in all lines of sight for which $A_V > 2.6$. This is, however, difficult to reconcile with the absence of substructure in the long-wavelength wing. The diffuse ISM features, and indeed most simple hydrocarbons studied in the laboratory, have relatively narrow, distinct features near 3.4 μm (see e.g. d'Hendecourt & Allamandola 1986), while the long-wavelength wing in Taurus is broad and featureless (at least at the spectral resolution of our observations, $\lambda/\Delta\lambda \sim 160$). One way around this difficulty, if the hydrocarbons are part of the grain cores and not simply mixed in the ice mantles, would be if an overlying H_2O ice layer could change or mask the substructure. However, Baratta & Strazzulla (1990) have investigated this very point, and their spectra of a H_2O ice layer on top of a hydrocarbon residue still shows pronounced structure near 3.4 μm.

One additional constraint on the material responsible for the long-wavelength wing comes from the fact that the long-wavelength wing and the H_2O ice band have the same threshold extinction ($A_V \sim 2.6$), and that this threshold is substantially different from that of CO ice ($A_V \sim 5.3$: Whittet et al. 1989). This is an argument in favour of the carrier of the long-wavelength wing being more refractory than CO ice, but, if the primary desorption mechanism near the cloud edges is photodesorption, the thresholds for molecular species more refractory than CO are probably not related to their evaporation temperatures, so further differentiation between species might not occur. If the carrier of the long-wavelength wing were the hydrocarbon material found in the diffuse ISM, however, it should be much more refractory than H_2O ice, and hence should remain on the grains after the H_2O ice has disappeared, yet this is not consistent with the existence of a threshold for the long-wavelength wing at $A_V \sim 2.6$, and is therefore an argument against the presence of a highly refractory hydrocarbon as a common component of the grains in Taurus.

In summary, although there is indirect evidence for hydrocarbons on grains in molecular clouds, there is a puzzling lack of substructure near 3.4 μm which would normally be expected from hydrocarbons. In addition, the existence of a threshold A_V for the long-wavelength wing is inconsistent with a highly refractory hydrocarbon giving rise to the wing.

5.4 Mantle photolysis

The question as to whether mantle photolysis is taking place in Taurus is linked to the question of the composition of the grain mantles (i.e. the existence of hydrocarbons), which has not yet been resolved. If we assume, however, that mantle photolysis involves the reaction of simple hydrocarbons like CH_4 and CH_3OH, which are *already present* in the grain mantles, to form more complex (i.e. more refractory) ones, a change in the absorbance (per C–H bond) of these molecules should be detectable in our data in the form of a change in the slope of the A_V versus $\tau_{3.45}$ relationship. In the laboratory, significant differences in the measured absorbances (per C–H bond) between different hydrocarbons are certainly seen (e.g. d'Hendecourt & Allamandola 1986), yet the strength of the long-wavelength wing at 3.45 μm relative to both A_V and the H_2O ice band strength does not change appreciably in our sample (Figs 4b and c). This of course depends on which molecules are present before and after photolysis and, more importantly, also assumes that the UV flux is higher on the dust in low-A_V lines of sight, which may not be the case if UV radiation can penetrate throughout the cloud because of a clumpy density structure – in this case the amount of photolysis would be essentially independent of A_V.

One might reasonably expect to detect any new spectral features arising because of photolysis at low A_V, at least in the early-type stars (photospheric features might make this more difficult in the late-type stars). Sandford et al. (1991) certainly see distinct hydrocarbon features near 3.4 μm in the diffuse ISM; however, from the strength that they estimate for this feature, $A_V/\tau_{3.432} \sim 240$, a similar feature in the *low-*A_V Taurus stars ($A_V < 5$) would be very near to the noise level of our spectra. Of course, once again, if the density structure in Taurus is clumpy, the amount of photolysis will be essentially independent of A_V and we would then expect to see distinct spectral features in the *high-*A_V stars – but again there is no indication of any distinct features (i.e. substructure) near 3.4 μm, at least above the noise level, in any of the Taurus spectra.

In summary, the present data are not able to resolve the question of whether photolysis of the icy grain mantles is *producing* refractory hydrocarbons in Taurus, but they do show that such refractory hydrocarbons are not a common component of these grains. In fact, considering this and the discussion in the preceding sections, there is no firm evidence for hydrocarbons (refractory or otherwise) on the grains in Taurus, either near the cloud edges or deep in the cloud interior. Notably absent is some indication of the molecule or molecules which might ultimately be expected to produce the diffuse ISM 3.4-μm feature, i.e. volatile hydrocarbons. The mantles appear to be dominated by H_2O ice, as evidenced by the consistency of the 3.05- and 3.45-μm thresholds, which leads us to speculate that the long-wavelength wing may be due to some non-hydrocarbon molecule (or molecules) complexed with the H_2O and therefore subject to the same mechanism(s) which govern the for-

mation and evolution of H_2O ice mantles on the grains. This would mean looking elsewhere for hydrocarbons. However, there is already evidence for another grain component, namely that containing the CO ice. A comparison between observations and laboratory spectra in Taurus (and other regions) has shown that most of the CO ice must reside in a component of the grain mantles that is dominated by non-polar molecules (i.e. *not* H_2O: see e.g. Tielens et al. 1991; Whittet & Duley 1991). Perhaps these non-polar molecules are the key to the whereabouts of the hydrocarbons in Taurus. Of course, there could also be two (or more) grain populations, one with H_2O ice dominated mantles and one with CO ice (or non-polar molecule) dominated mantles. It is interesting in this regard that the presence or absence of CO ice on the grains has no noticeable effect on the long-wavelength wing or H_2O ice band strengths. In any event, what is revealed is a picture of the grain mantles that is significantly more complex than a few simple molecules mixed with H_2O, and one that we are not able to clarify with the evidence at hand.

6 CONCLUSIONS

Based on a careful study of the absorption features near 3 μm in the spectra of a sample of field stars lying behind the Taurus dark cloud, we draw the following conclusions.

(i) An abnormal extinction law for several of the Taurus field stars (i.e. $R \sim 3.5$–3.7) leads us to adopt the relation $A_V = 5.4E(J-K)$ to derive A_V for all of those stars in our sample that are definitely reddened by material in the cloud.

(ii) An absorption feature is found near 2.96 μm in the spectra of several of the late-type stars in the sample. Because this feature is absent from the spectra of the early-type stars, and its strength increases with increasing spectral type in the late-type stars, we attribute it to a photospheric feature intrinsic to the late-type stars; it definitely does not arise in material in the Taurus cloud.

(iii) Very good correlations exist between A_V and the H_2O ice absorption ($\tau_{3.05}$), yielding $\tau_{3.05}/A_V = 0.059 \pm 0.003$, and between A_V and the strength of the long-wavelength wing ($\tau_{3.45}$), yielding $\tau_{3.45}/A_V = 0.0077 \pm 0.0005$. In addition, both H_2O ice and the long-wavelength wing have the same threshold extinction, $A_{V_0} = 2.6$. After examining several possible desorption mechanisms, we conclude that photodesorption is sufficient to explain the H_2O ice threshold (and probably also the long-wavelength wing threshold). The constancy of $\tau_{3.05}/A_V$ implies that photodesorption operates throughout the cloud, and thus that UV photons penetrate throughout the cloud; this could be explained by a clumpy cloud structure. The long-wavelength wing threshold argues against the wing arising from a highly refractory hydrocarbon material like that found in the diffuse ISM.

(iv) By fitting the H_2O ice absorption with a model employing graphite and silicate grain cores that follow an MRN size distribution, coated with a layer of amorphous H_2O ice, and taking into account all of the observational constraints, we find two possible scenarios for the distribution of ice mantles on the grains in Taurus. Either (1) the grains have a variable mantle thickness, with most of the ice on the larger grains, or (2) there are two grain populations in Taurus, one comprising bare grains and the other comprising thick ($a_{th} = 0.35$ μm) ice-coated grains, in the approximate ratio 3×10^4:1. Both scenarios yield an oxygen depletion (in the form of H_2O ice) for Taurus in the range 8–9 per cent.

(v) Photodesorption seems sufficient to explain the existence of the H_2O ice and long-wavelength wing thresholds and, if we combine this with a clumpy cloud structure, we have a logical explanation for the bare/mantled grain mixture. The simplicity of this explanation and its agreement with all of the observations make it appealing as a description of the physical environment in the Taurus dark cloud.

(vi) While hydrocarbons remain the most likely explanation for the long-wavelength wing, there are difficulties with this proposal, in particular the lack of substructure in the wing. Similarly, the lack of distinct hydrocarbon features creates difficulties with the proposition that mantle photolysis is taking place in Taurus. This leaves us with no direct evidence for either hydrocarbons on grains or mantle photolysis in dark clouds, so the question is far from settled.

What is definitely required is more laboratory work on hydrocarbon mixtures to discover whether the featureless long-wavelength wing can be reproduced, and the effects of photolysis on such a mixture (i.e. whether it produces substructure like that seen in the diffuse ISM). Observationally, spectra with both higher resolution and higher signal-to-noise ratio of 3-μm ice features in Taurus and other dark clouds are clearly very desirable, particularly at low A_V where evidence for photolysis might be expected.

ACKNOWLEDGMENTS

The authors thank the staff of the Infrared Telescope Facility for their very able assistance in preparing the instrument and in obtaining the observations described here. We thank Y. Pendleton for permission to use the spectrum of V842 Aql in advance of publication. RGS was at the University of California, Irvine, and KS and TYB were at the Institute for Astronomy, University of Hawaii, during the initial phases of this work. KS and TYB gratefully acknowledge partial support from NASA contract NASW-3159.

REFERENCES

Allen C. W., 1973, Astrophysical Quantities, 3rd edn. Athlone Press, London
Baratta G. A., Struzulla G., 1990, A&A, 240, 429
Bazell D., Dwek E., 1990, ApJ, 360, 142
Beer R., Hutchison R. B., Norton R. H., Lambert D. L., 1972, ApJ, 172, 89
Boland W., de Jong T., 1982, ApJ, 261, 110
Crutcher R. M., 1985, ApJ, 288, 604
d'Hendecourt L. B., Allamandola L. J., 1986, A&AS, 64, 453
d'Hendecourt L. B., Allamandola L. J., Baas F., Greenberg J. M., 1982, A&A, 109, L12
Dickman R. L., Horvath M. A., Margulis M., 1990, ApJ, 365, 586
Draine B. T., 1985a, in Black D. C., Matthews M. S., eds, Protostars and Planets II. Univ. of Arizona Press, Tucson, p. 621
Draine B. T., 1985b, ApJS, 57, 587
Draine B. T., Lee H. M., 1984, ApJ, 285, 89
Draine B. T., Salpeter E. E., 1979, ApJ, 231, 438
Duley W. W., Williams D. A., 1981, MNRAS, 196, 269
Elias J. H., 1978, ApJ, 224, 857

Frogel J. A., Persson S. E., Aaronson M., Matthews K., 1978, ApJ, 220, 75
Graham J. A., Chen W. P., 1991, AJ, 102, 1405
Greenberg J. M., 1973, in Gordon M. A., Snyder L. E., eds, Molecules in the Galactic Environment. Wiley, New York, p. 93
Greenberg J. M., 1982, in Beckman J. E., Phillips J. P., eds, Submillimetre Wave Astronomy. Cambridge Univ. Press, Cambridge, p. 261
Hagen W., Tielens A. G. G. M., Greenberg J. M., 1981, Chem. Phys., 56, 367
Johnson H. L., 1968, in Middlehurst B. M., Aller L. H., eds, Stars and Stellar Systems, Vol. 7, Nebulae and Interstellar Matter. Univ. Chicago Press, Chicago, p. 193
Kitta K., Krätschmer W., 1983, A&A, 122, 105
Léger A., Gauthier S., Defourneau D., Rouan D., 1983, A&A, 117, 164
Léger A., Jura M., Omont A., 1985, A&A, 144, 147
Mathis J. S., Wallenhorst S. G., 1981, ApJ, 244, 483
Mathis J. S., Whiffen G., 1989, ApJ, 341, 808
Mathis J. S., Rumpl W., Nordsieck K. H., 1977, ApJ, 217, 425 (MRN)
Merrill K. M., Russell R. W., Soifer B. T., 1976, ApJ, 207, 763
Merrill K. M., Stein W. A., 1976, PASP, 88, 285
Nakagawa N., 1980, in Andrew B. H., ed., Interstellar Molecules. Reidel, Dordrecht, p. 365
Sandford S. A., Allamandola L. J., 1988, Icarus, 76, 201
Sandford S. A., Allamandola L. J., Tielens A. G. G. M., Sellgren K., Tapia M., Pendleton Y. J., 1991, ApJ, 371, 607
Scargle J. D., Strecker D. W., 1979, ApJ, 228, 838
Schutte W., Greenberg J. M., 1986, in Israel F. P., ed., Light on Dark Matter. Reidel, Dordrecht, p. 229
Sellgren K., 1990, in Bussoletti E., Vittone A. A., eds, Dusty Objects in the Universe. Kluwer, Dordrecht, p. 35
Smith R. G., Sellgren K., Tokunaga A. T., 1989, ApJ, 344, 413
Snell R. L., Heyer M. H., Schloerb F. P., 1989, ApJ, 337, 739
Straižys V., Meištas E., 1980, Acta Astron., 30, 541
Straižys V., Wisniewski W. Z., Lebofsky M. J., 1982, Ap&SS, 85, 271
Straižys V., Černis K., Hayes D. S., 1985, Ap&SS, 112, 251
Strecker D. W., Erickson E., Witteborn F. C., 1979, ApJS, 41, 501
Stutzki J., Stacey G. J., Genzel R., Harris A. I., Jaffe D. T., Lugten J. B., 1988, ApJ, 332, 379
Tamura M., Nagata T., Sato S., Tanaka M., 1987, MNRAS, 224, 413
Tanaka M., Sato S., Nagata T., Yamamoto T., 1990, ApJ, 352, 724
Tielens A. G. G. M., Tokunaga A. T., Geballe T. R., Baas F., 1991, ApJ, 381, 181
Tokunaga A. T., Brooke T. Y., 1990, Icarus, 86, 209
Tokunaga A. T., Smith R. G., Irwin E., 1987, in Wynn-Williams C. G., Becklin E. E., eds, Infrared Astronomy with Arrays. Univ. Hawaii, Honolulu, p. 365
Ungerechts H., Thaddeus P., 1987, ApJS, 63, 645
van de Bult C. E. P. M., Greenberg J. M., Whittet D. C. B., 1985, MNRAS, 214, 289
Vrba F. J., Rydgren A. E., 1985, AJ, 90, 1490
Watson W. D., Salpeter E. E., 1972a, ApJ, 174, 321
Watson W. D., Salpeter E. E., 1972b, ApJ, 177, 659
Whittet D. C. B., 1992, in Tayler R. J., White R. E., eds, The Graduate Series in Astronomy: Dust in the Galactic Environment. IOP Publishing, London, p. 158
Whittet D. C. B., Duley W. W., 1991, A&AR, 2, 167
Whittet D. C. B., van Breda I. G., 1980, MNRAS, 192, 467
Whittet D. C. B., Bode M. F., Longmore A. J., Baines D. W. T., Evans A., 1983, Nat, 303, 218
Whittet D. C. B., Longmore A. J., McFadzean A. D., 1985, MNRAS, 216, 45P
Whittet D. C. B., Bode M. F., Longmore A. J., Adamson A. J., McFadzean A. D., Aitken D. K., Roche P. F., 1988, MNRAS, 233, 321
Whittet D. C. B., Adamson A. J., Duley W. W., Geballe T. R., McFadzean A. D., 1989, MNRAS, 241, 707
Wickramasinghe N. C., 1967, in Interstellar Grains. Chapman and Hall, London, p. 57
Williams D. A., Hartquist T., Whittet D. C. B., 1992, MNRAS, 258, 599